J Nanopart Res (2015) 17:389
DOI 10.1007/s11051-015-3187-y

RESEARCH PAPER

Polyaniline nanoparticles for near-infrared photothermal destruction of cancer cells

Edith Inés Yslas · Luis Exequiel Ibarra · María Alejandra Molina · Claudia Rivarola · Cesar Alfredo Barbero · Mabel Lucía Bertuzzi · Viviana Alicia Rivarola

Received: 11 May 2015 / Accepted: 18 September 2015

Abstract Polyaniline nanoparticles (PANI-Nps) have been used in several applications; however, there are few publications related to the use in the photothermal therapy. PANI-Nps have high optical absorbance in the near-infrared region and in this wavelength range, biological systems are relatively transparent. For this reason, these materials can be used to absorb energy and to generate heat that destroys cancer cells selectively. PANI-Nps with average size of ca. 200 nm and neutral zeta potential were synthesized and characterized by DLS, SEM, and zeta potential. The kinetics of incorporation of PANI-Nps into LM2 cell line was monitored using UV–Vis spectrophotometry. The analysis of cell viability after PANI-Nps exposure shows that these nanoparticles are not cytotoxic even at high concentration and show no change in cell morphology and metabolic activity. Furthermore, we found that nanoparticle cell uptake reaches the maximum value c.a. 3 h after incubation. Cells were targeted by Pani-Nps and irradiated, resulting in significant elevation of intracellular ROS and heat production. One of the mechanisms of PANI-Nps-mediated photothermal killing of cancer cells apparently involved oxidative stress resulting in apoptotic cell death.

Keywords Polyaniline nanoparticles · Cytotoxicity · Nanomedicine · Cancer · Photothermal therapy · Environmental and health effects

Edith Inés Yslas and Luis Exequiel Ibarra have contributed equally.

E. I. Yslas (✉) · L. E. Ibarra · M. L. Bertuzzi · V. A. Rivarola (✉)
Departamento de Biología Molecular, Universidad Nacional de Río Cuarto, Agencia Postal Nro3, X580BYA Río Cuarto, Argentina
e-mail: inesilla.yslas@gmail.com

V. A. Rivarola
e-mail: vrivarola@exa.unrc.edu.ar

M. A. Molina · C. Rivarola · C. A. Barbero
Departamento de Química, Universidad Nacional de Río Cuarto, Agencia Postal Nro3, X580BYA Río Cuarto, Argentina

Introduction

The effectiveness of a cancer therapeutic device is measured by its ability to reduce and eliminate tumors without damaging healthy tissue. A revolution in cancer therapy has evolved with the emerging use of laser light to achieve controlled and confined thermal damage in the tumor tissue (Welch 1984). Nanotechnology is currently offering alternative techniques for remote and localized heating that are based on the development and bioincorporation of heating nanoparticles. In addition, nanoparticles have been widely considered for various applications such as the development of drug and gene delivery system (Kievit et al. 2009; Wang et al. 2011a), tissue engineering (Shevach

Published online: 30 September 2015

et al. 2014), and cellular imaging (Fery-Forgues 2013). Photothermal therapy (PTT) has been widely studied as a minimally invasive treatment modality in comparison with other methods (Sultan 1990; Jaque et al. 2014). The PTT has many advantages over other photo-assisted therapies. From a clinical perspective, cancer cells are generally more sensitive to the heat than normal cells due to the lack of an efficient cooling system supplied by abnormal blood vessels, which induces damage and apoptosis to the cancer cells (Kampinga 2006). In this type of therapy, the light in the near-infrared wavelength range (NIR), between 700 and 1200 nm, is more useful than UV–Vis light since it is less absorbed by live tissue. This is due to the fact that few biological chromophores and water barely absorb light in the NIR region, and thus light can penetrate deeper into biological tissues (Weissleder 2001), and due the advantage conferred entirely by nanomaterials. Moreover, it is widely accepted that nanoparticles can be easily absorbed by cells (Thurn et al. 2011; Sokolova et al. 2013). For this reason, a variety of nanoparticle systems are currently being explored for cancer therapeutics (Haley and Frenkel 2008), which include dendrimers (Zhao et al. 2014), liposome (Allison 2007; Bovis et al. 2012), micelles (Lee et al. 2003), carbon nanotubes (Huang et al. 2010), and polymeric nanoparticles (Kumari et al. 2010; Li and Liu 2014). Several nanoparticles based on organic and inorganic chromophores, which show strong absorption in the near-infrared (NIR) tissue-transparency window, such as gold and carbon nanomaterials, have displayed encouraging photothermal therapeutic efficacy in preclinical animal experiments (Yuan et al. 2012; Chu et al. 2013). However, the major issue with these types of nanomaterials is their low biocompatibility, particularly their long-term toxicity, which limits their clinical application (Balasubramanian et al. 2010; Zhang et al. 2011). Recently, we have demonstrated that polyaniline nanoparticles are very effective for in vivo photothermal therapy, and have nontoxic effects and a good tolerance (Ibarra et al. 2013, 2015). Polyaniline is one of the most promising conducting organic polymers because of its low cost, facile synthesis, high conductivity, and environmental and chemical stabilities (Heeger 1993; Stejskal and Sapurina 2005; Stejskal and Proke 2014). This polymer is a well-studied system having large number of applications in nanoelectronics (Novák et al. 1997), inkjet printing (Ngamna et al. 2007), optoelectronics, photonics, chemical, and electrochemical sensors (Virji et al. 2004) and biology (Yslas et al. 2012; Stejskal et al. 2014). Polyaniline has a high optical absorbance in the NIR region, where NIR light achieves the highest tissue penetration. Moreover, polyaniline is noncytotoxic and has been successfully used as an electroactive material for studying cellular proliferation and in the field of nanomedicine (Li et al. 2009; Yang et al. 2011; Villalba et al. 2012). In the present study, the ability of an organic conducting polymer to be employed in photothermal therapy is analyzed evaluating PANI-Nps toxicity, the cell uptake, and its ability to promote tumor cell death by photothermic effect, thus revealing a possible mechanism of cell death.

Materials and methods

Synthesis and characterization of PANI-Nps

Polyaniline nanoparticles were synthesized by nucleation and growth polymerization, using poly(vinylpyrrolidone) as stabilizer (Stejskal and Sapurina 2005). Aniline hydrochloride (259 mg) was dissolved in an aqueous solution of 40 g/L of poly(N-vinylpyrrolidone) (PVP Fluka, Mn = 360,000), instead of water, to 5 mL of solution. Polymerization was started at 20 °C by adding 5 mL of aqueous solution containing 571 mg of ammonium peroxydisulfate. The mixture was briefly stirred and left at rest to polymerize. The polymerization was finished in several minutes. PANI-Nps formed a stable suspension at physiological pH. The total amount of PANI-Nps in the obtained dispersion was calculated from the concentration and volume. Then, the mass of PANI-Nps was rationed with the mass of the reactants (aniline hydrochloride, PVP, and persulfate) to calculate a percentage yield of the synthesis. The diameters of PANI-Nps were characterized by dynamic laser light scattering (DLS) and scanning electron microscopy (SEM). In addition, these nanoparticles were characterized by zeta potential and electronic properties analyzed by UV–Vis spectra.

Heat production by NIR light absorption

PANI-Nps dispersed in water were placed in glass tubes with magnetic stirring and covered with a

polystyrene box to avoid heat leakage. A solid-state NIR laser (Ocean Optics), which emits light, (785 nm, 500 mW) was guided through an optical fiber the end of which was placed at 2 cm over the liquid/air interface. The temperature was measured using a TES 1326S/1327K infrared thermometer after irradiation pulses (Hong et al. 2011; Fu et al. 2012).

Cell culture

Cell culture experiments were carried out using murine mammary adenocarcinoma cell line (LM2) purchased from Hospital Roffo (Buenos Aires, Argentina), and for biocompatibility analysis, Human keratinocyte cell line (HaCaT) and murine colonic carcinoma cell line (CT26.WT) were also used. Cells were grown in medium Dulbeccós modified Eaglés medium (DMEM) supplemented with 10 % fetal bovine serum (Sigma); 2 mM L-glutamine, 100 mg/mL penicillin G, and 100 mg/mL streptomycin (Gibco) at 37 °C in a humidified and 5 % CO_2 atmosphere (Hera Cell, Thermo Scientific, Waltham, MA).

Uptake of PANI-Nps into live cells

Cellular nanoparticles uptake was determined by UV–Vis spectroscopy, using the optical absorption of polyaniline in solution. Cells were seeded (5.0×10^5) into 60-mm culture dishes in 4 mL of DMEM containing 10 % fetal bovine serum and then incubated overnight at 37 °C. Afterward, the cells were incubated in the dark at 37 °C for various time intervals (0–24 h) with 4 mL of DMEM containing 10 % FBS and 0.42 or 1.04 mg/mL PANI-Nps.

Cells were washed twice with PBS and harvested using a cell scraper. The cell number per mL was calculated by using a hemocytometer chamber (Improved Neubauer). Subsequently, the intracellular concentration of PANI-Nps was calculated considering the cell number after the incubation time of each treatment group. Cells were lysed by addition of 4 % aqueous sodium dodecyl sulfate (SDS) to 1 mL of cellular suspension and after centrifugation; 1 mL of buffer (sodium acetate/acidic acid, 0.1 M) was added to the supernatant to dissolve the polyaniline and to preserve pH of samples. To determinate PANI-Nps' concentration, a calibration curve was obtained with stock solution. To this end, 4 aliquots of 500 μL of the stock PANI-Nps solution were dehydrated, at reduce pressure in a vacuum oven in a preweighed recipient. The mass of the obtained solid residue was calculated and used to estimate the average concentration (mg/mL) of PANI-Np in the stock solution. A calibration curve was constructed as follows. Different volumes of PANI-Nps stock solution were diluted into 5 mL of buffer (sodium acetate/acidic acid, 0.1 M). The absorptions of the resulting dilutions were measured at 636 nm, and the absorbances were plotted as a function of the PANI-Nps' concentration. The calibration curve showed a lineal relationship with a slope of ~ 2.99 cm^3 mg^{-1} cm^{-1}.

Inhibition of endocytosis

For the temperature-dependent effects on uptake, cells were preincubated for 1 h at either 4 or 37 °C before and during the treatment with nanoparticles. The cells were treated with PANI nanoparticles (1.04 mg/mL) for 0.5 and 1 h and finally processed as per the previous experiment to determine the concentration of nanoparticles in cells.

Cytotoxicity in dark condition of PANI-Nps on LM2 cells

Nanoparticle cytotoxicity was assessed by different colorimetric cell viability assays: the 3-(4,5-dimethylthiazol)-2-diphenyltetrazolium bromide (MTT) test, neutral red uptake, and tripan blue stain. These experiments were carried out employing different tumor cell lines (LM2 and CT26) and a normal cell line (HaCat). The MTT assay was conducted to assess cellular viability based on mitochondrial function. Ability of viable cells to incorporate and bind the supravital dye neutral red in the lysosomes was also performed. To this end, cells were seeded into 96-well microplates at a concentration of 200,000 cell/mL and allowed to grow for 24 h to a subconfluent state, the culture medium was replaced with fresh medium containing different PANI nanoparticles concentrations.

MTT assay was performed culturing cells with suspended nanoparticles (0.42–12 mg/mL) for 24 h. MTT solution (5 mg/mL in culture medium) was added (final concentration 0.5 mg/mL), and cells were incubated for 3 h at 37 °C in 5 % CO_2 before the analysis. Thereafter, the medium was removed, and 200 μL DMSO was added to dissolve blue formazan crystals. A purple color developed within the cells,

indicating the cleavage of the tetrazolium salt (MTT) by mitochondrial reductase in live cells. The absorbance of the formed dye was measured at 550 nm using a microplate reader. Absorbance values for untreated wells were taken as control reference (100 % survival).

Concerning the neutral red assay, following exposure to PANI-Nps (24 h), cells were incubated for 2 h with neutral red dye (100 μg/mL) dissolved in serum-free medium (DMEM). Cells were then washed with phosphate buffered saline (PBS) and 1 mL of elution medium (EtOH/AcCOOH, 50/1 %) was added, followed by gentle shaking for 10 min so that complete dissolution was achieved. The absorbance of neutral red dye was measured at 540 nm using a microplate reader. Absorbance values for untreated wells were taken as control reference (100 % survival).

In addition, after incubation with nanoparticles at different times (0–24 h), medium was removed, and cells were washed with PBS twice and harvested using a cell scraper. Cell suspensions were counted via hemocytometer with Trypan blue staining. This method evaluated membrane integrity and allowed counting nonviable cells since only those cells admit blue staining into the cell. All experiments were run in triplicate.

To confirm the cell viability after nanoparticles' exposure, a clonogenic assay or colony-formation assay was performed with LM2 cells. The assay essentially tests every cell in the population for its ability to undergo ''unlimited'' division. First, cells were seeded into 35 mm Petri dishes at a concentration of 200,000 cell/mL to a subconfluent state. Afterward, cells were incubated for 24 h with the suspended nanoparticles (0.42–12 mg/mL) and then, the medium was removed, and the cells were washed with PBS. They were trypsinized to produce a single-cell suspension, were plated at a very low density in p-35 dishes (200 cells per dish), and allowed to grow until colonies were observed (10 days). The colonies were defined to consist of at least 50 cells. Finally, these cells were fixed with methanol and stained with Methylene Blue to proceed with the counting of colonies. It is assumed that each colony originates from a single plated cell.

Laser treatment of tumor cells with PANI-Nps

To evaluate the effect of PTT with PANI-Nps, LM2 cells were incubated for 3 h with PANI-Nps' suspensions in DMEM (0.42 and 1.02 mg/mL), the time when PANI-Nps reached a maximum concentration inside the cells. After removing the medium, two washings with PBS were performed, and fresh medium was added. Subsequently, cells were irradiated with continuous NIR light from a laser Raman System Inc. LED (785 nm) at a light intensity of 500 mW/cm^2 for 5–15 min. The laser spot has a diameter of 2 mm approximately. The same procedure was performed in the absence of light as a control of PANI-Nps in darkness. As an irradiation control, cells were irradiated as described above, but without the addition of PANI-Nps in medium. The polymer dispersant of nanoparticles combined with irradiation was also evaluated. To this end, cells were incubated with dispersant solution in medium at the same concentration used with nanoparticles following the same protocol described above. The morphology of cells, on the irradiation area, was determined using Toluidine blue staining and optical microscopy and atomic force microscopy (AFM).

AFM procedure

AFM measurements were made using an Agilent 5420 AFM/STM microscope under ambient conditions. The analysis of fixed cells was carried out at room temperature (20−25 °C) using a commercial Point Probe® Plus Non-Contact/Tapping Mode-Long Cantilever (PPP-NCL) with a force constant of 6 N m^{-1} and resonance frequency of 156 Hz in the Acoustic AC (AAC) mode.

Determination of oxidative stress after PANI nanoparticles exposure and PTT

Taking into account that nanomaterials can induce oxidative stress on their own, as well as trying to figure out its implications after photothermal therapy, the oxidative stress triggered by PANI-Nps was assayed. To this purpose, the diacetate probe 2′,7′-dichlorodihydrofluorescein (DCFH-DA) was used. This is one of the most widely used techniques to measure directly the redox state of cells (Royall and Ischiropoulos 1993). DCFH-DA is a nonfluorescent precursor to dichlorofluorescein (DCF). This nonfluorescent molecule accumulates in the cells and in the presence of ROS generates DCF, a highly fluorescent product. Before incubation of monolayer cultures with different PANI-Nps dispersions, the incubation of the cells was carried out with 10 μM solution of DCFH-

DA in PBS for 1 h. Then, cells were washed with PBS and were subjected to two PANI-Nps concentrations (0.42 y 1.04 mg/mL) for 3 h to be subsequently exposed to photothermal treatment with PANI-Nps. Finally, we proceeded to observe the cells under fluorescence microscope after PTT. The different treatment groups consisted of only irradiated cells; cells treated with the dispersant of the PANI-Nps (PVP) un-irradiated and irradiated cells; cells incubated with PANI-Nps (0.42 y 1.04 mg/mL) without irradiation; cells without any treatment; and positive control cells incubated with 100 μM H_2O_2.

Results and discussion

Characterization of PANI-Nps

The size and shape of the PANI nanoparticles were characterized by SEM (Fig. 1a) and DLS. Also Zeta potential was obtained (Fig. 1b). SEM image shows very uniform and spherical nanoparticles with an average size of 200 nm c.a. The size of the nanoparticles measured by DLS was similar to SEM analysis with an average size of 224 nm and a polidispersant index (PII = 0.145) showing uniform monodispersity of samples. The yield of the synthesis described in this work was of 77 ± 0.1 % (data not shown).

Figure 1c shows the UV–Vis spectra of PANI-Nps in acid-doped state at pH = 5 (solid line). At pH 7, PANI-Nps were in base undoped state (denoted by dot line). In the spectrum at pH = 7, it is possible to observe the three characteristic bands at ca. 290, ca. 366, and ca. 627 nm of the PANI-Nps. At pH 5, it is also possible to recognize the three characteristic bands at ca. 320, ca. 430, and ca. 780 nm. The shoulder at ca. 320 nm is attributed to the $\pi \rightarrow \pi^*$ transition of the aniline ring, and the band at ca. 430 nm is assigned to the $n \rightarrow \pi^*$ transition of the localized radical cation. Moreover, the band at ca. 780 nm is assigned to the excitation from the highest occupied molecular orbital (HOMO) of the benzenoid rings (pb) to the lowest unoccupied molecular orbital (LUMO) of the quinoid rings (pq) in the quinoneimine units. This behavior is characteristic of conductive and electroactive PANI (Acevedo et al. 2007).

Since PANI in an acid media absorbs light in the NIR range (700–1200 nm) and taking into account that various solid tumors (adenocarcinoma, squamous cell carcinoma, soft tissue sarcoma, and malignant melanoma) have a pH range between 5.7 and 7.8 (Lee et al. 2003, 2008), it is possible to heat PANI-Nps by irradiation with NIR light.

Figure 1d shows the temperature change (ΔT (°C) = Tf − Trt) from room temperature (Trt) to that upon application of radiation (Tf). The temperature changes of different PANI-Nps concentration were tested after irradiation with NIR laser light for 15 min. A PANI-Nps' dispersion of 0.167 mg/mL produces a significant increment of 3.5 °C, and a PANI-Nps' dispersion of 0.313 mg/mL in acid solution causes an increment of ca. 4 °C, the same as for the dispersion of 0.419 mg/mL. However, a major concentration (1.04 mg/mL) increases the temperature to more than 12 °C. The increase of temperature achieved in the surrounding medium of nanoparticles was significant compared with the water control in all the concentrations tested.

In vitro cellular uptake

The biokinetics of nanoparticles, which is measured as the rate of nanoparticle uptake, is expected to make a large contribution to their toxicity. *In vitro* determinations of intracellular drug accumulation indicate that PANI-Nps are taken up by LM2 cells at low incubation times (<3 h). Then, it leads to a saturation value at incubation time of c.a. 3 h. The uptake is estimated to be 0.07 mg/10^6 cells when the cultures were treated with 0.42 mg/mL of PANI-Nps. Similar uptake profile was observed when Nps concentrations were 1.04 and 0.42, reaching a plateau value of 0.33 mg/10^6 cells at a low incubation time of 3 h (Fig. 2a). Consequently, it is possible to conclude that cellular uptake increases with the increasing nanoparticles' concentration exposure.

In addition, in order to investigate the effect of cellular metabolism on the uptake of PANI-Nps, cells were incubated at 4 °C before and during the treatment with nanoparticles (Fig. 2b). LM2 cells were treated with 1.04 mg/mL PANI-Nps for 0.5 and 1 h at either 4 or 37 °C, and the intracellular concentration of nanoparticles determined by UV–Vis spectroscopy. Uptake at 37 °C was similar to previous experiments, but it diminished 60 % in cells treated at 4 °C compared to 37 °C. This result suggests an active endocytic mechanism of nanoparticle incorporation. However, the inhibition of endocytosis was not

A

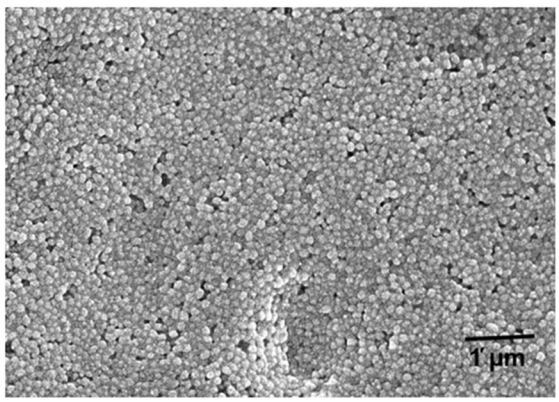

B

DLS (nm)	PdI	Zeta-Potential (mV) pH= 5
224	0.145	-7.58 ± 0.54

C

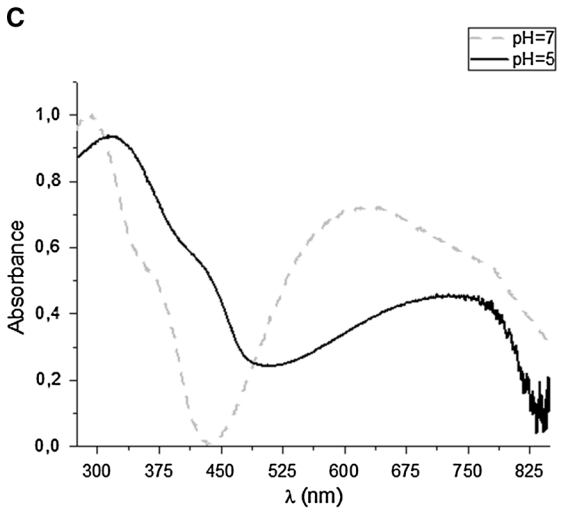

D

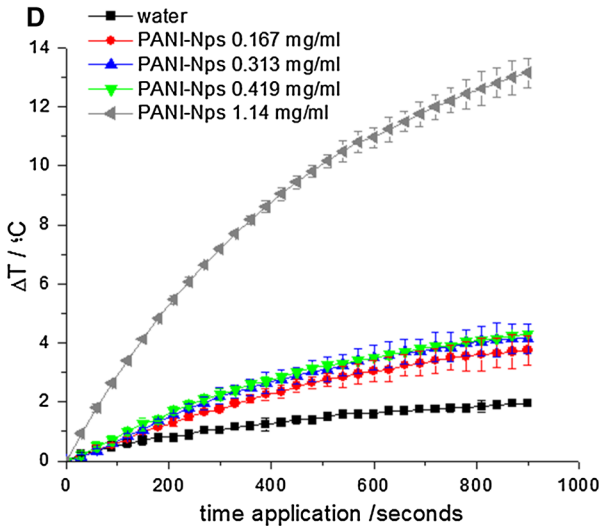

Fig. 1 **a** SEM micrographs of PANI-Nps, **b** Hydrodynamic diameter (DLS) and Zeta-potential of dispersed PANI-Nps, **c** UV–Vis spectra of PANI nanoparticles at different pH, and **d** temperature variation (ΔT) of PANI-Nps' dispersion by NIR laser application at different times

completed; probably some of the nanoparticles remain attached to the cell membrane. Casas et al. have shown that, in explants treated with liposomal ALA, phospholipid vesicles can be seen in the cytoplasm, and they can also be seen in the intracellular space after being incorporated into the cell. The presence of huge lisosomes containing liposomes is evidence enough to show the participation of the endocytic pathway in the release of the entrapped ALA into the LM2 cell line (Casas et al. 2002).

The lysosomal compartment has been suggested to be the most probable intracellular site of storage and degradation of nanomaterials (Stern et al. 2012). This organelle presents an acidic pH (4–5.5), and for this reason, the polyaniline triggers transition state from an emeraldine base (EB) to an emeralidine salt (ES). This phenomenon occurs due to the increment of proton concentration influencing the conductivity of polyaniline (Choi et al. 2014). The only electrically conducting form is ES, as the EB/ES transition takes place mainly between pH 3 and 6, which suggests that the lysosomal pH improves its photothermal activity.

Many other nanoscale macromolecules and molecular assemblies are internalized through endocytosis. This endocytic fate of nanomaterials has been demonstrated by various precedents in the literature (Verma and Stellacci 2010). The shapes and sizes of nanoparticles have been found to greatly affect their cellular uptake process. The clathrin-mediated pathway of endocytosis shows an upper size limit for internalization

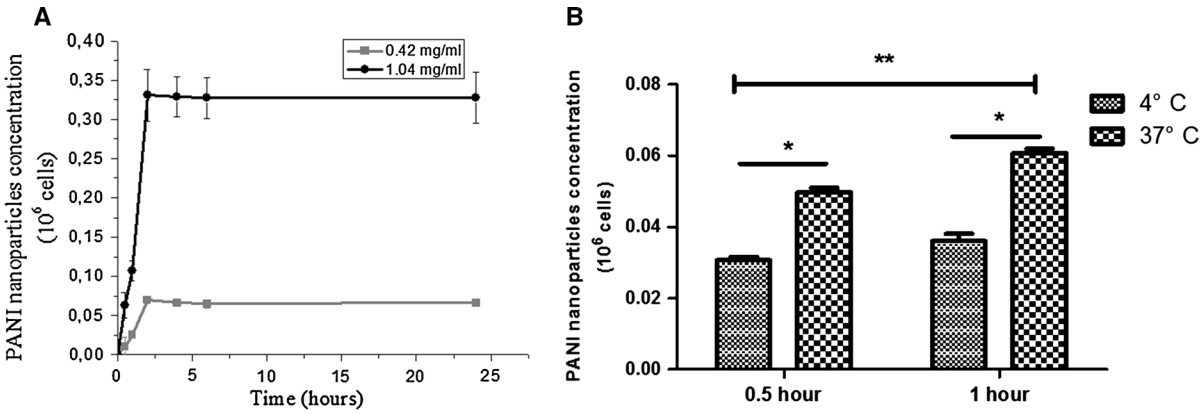

Fig. 2 Time course of PANI-Nps uptake: **a** PANI-Nps 0.42 or 1.04 mg/mL into LM2 cells as a function of incubation time at 37 °C. Values represent mean ± standard deviation of three separate experiments. **b** Effect of temperature on the rate of internalization of PANI-Nps into LM2 cells employing a concentration of 1.04 mg/mL

of approx. 200 nm, and kinetic parameters may determine the almost exclusive internalization of such particles along this pathway rather than via caveolae. Accordingly, these data suggest that, in a size-dependent manner, differences exist in the potential control and mechanism of internalization, a point of inflection becoming apparent at a size of approx. 200 nm where PANI-Nps has its mean size distribution.

Biocompatibility of PANI-Nps

Although the potential toxicity of the PANI nanoparticles was tested, it is important to evaluate its cytotoxicity using different methods. Viability assays assess the overall dose-dependent toxicity of PANI-Nps on cultured cells, testing different cell organelles. The MTT metabolic assay for cytotoxicity, which is a colorimetric assay that measures the enzymatic activity of cellular mitochondria, was employed. If cells properly metabolize the MTT dye, the cell culture will turn blue, allowing quantifying cellular activity by absorbance measurements (Marquis et al. 2009). Cell viability was also evaluated by the uptake of Neutral Red dye and binding to lysosomes. This assay represents the functionality of these organelles. Cell viability was significantly reduced in a dose-dependent manner after exposure to nanoparticles in all cell types (LM2, CT26, and HaCaT) tested by MTT and Neutral Red assays. However, the toxicity varied according to the test, showing different sensitivities (Fig. 3). This variation of sensitivity relates to the tested cell functions. For instance, PANI-Nps seem to cause a larger injury to mitochondria compared to the damage against lysosomes. In the case of LM2 cells, the LC50 determined by MTT is 7.5 mg PANI-Nps/mL; compared to the LC50 of 11.8 mg/mL determined by Neutral Red assay. These results were found at very high concentrations compared with other PANI nanomaterials with toxic effects at concentration starting of 1 and 100 μg/mL, respectively (Villalba et al. 2012; Kucekova et al. 2014). These differences could be attributed to modifications in nanoparticle's composition and properties like the shape and size. PANI nanoparticles, evaluated by Kucekova et al., were synthetized using a solution of PVP more concentrated (4 wt%) compared to our work (2 wt%). In a previous study, using an in vivo toxicological model to assays PANI-Nps exposure, we demonstrated that nanoparticle's toxicity was associated with the polymer stabilizer PVP concentration employed. This effect was not observed when a combination of polymers (PVP and PNIPAM, both with a concentration of 1 wt%) was used in PANI-Nps' synthesis (Ibarra et al. 2015). On the other hand, a major toxicity reported by Villalba et al. was dependent on the size and shape. It is well known that particle size and surface area play a major role in the interaction of materials with biological system. Apparently, the decreasing size of the materials leads to an exponential increase in surface area relative to volume, thereby making the nanomaterial's surface to be more reactive. In our previous study, we demonstrated a size-dependent toxicity of PANI-Nps in larvae of *R. arenarum* (Ibarra et al. 2015).

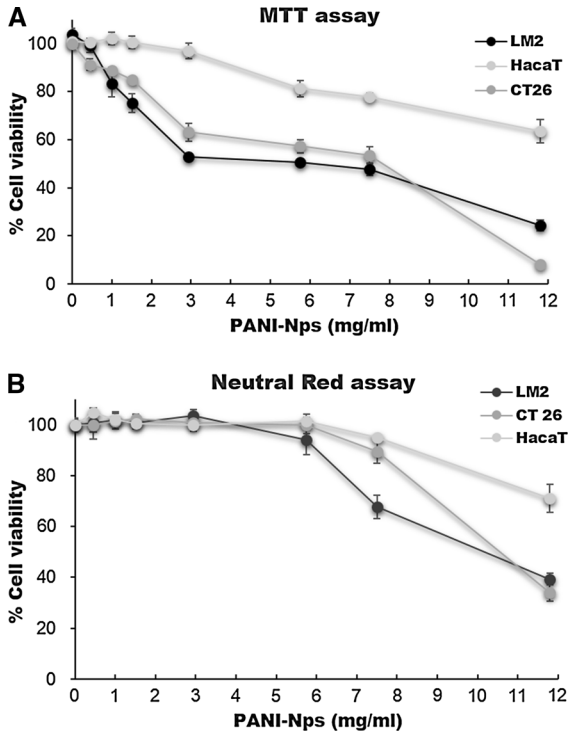

Fig. 3 Effects of PANI-Nps concentrations on cell viability after a 24-h exposure time: **a** MTT metabolism and **b** neutral *red* uptakes of LM2, CT26, and HaCaT cells under dark condition. Values are expressed as mean ± standard deviation of three separate experiments

HaCaT, a nontumor cell line, was more resistant to PANI-Nps' cytotoxicity, and therefore, it seems that tumor cells (LM2 and CT26), due to a higher metabolic rate and endocytic activity, could internalize more nanoparticles than normal cells and be more susceptible to exposure to PANI-Nps.

Another factor worth considering is that nanoparticles are capable of interacting with assay components or interfering with detection systems, resulting in unreliable data (Schulze et al. 2008). In order to reveal which assay adequately represents the cell viability after PANI Nps' exposure, a clonogenic analysis was performed (Fig. 4a). This assay is based on the ability of a single cell to grow into a colony after receiving nanoparticles' treatment. PANI-Nps' exposure at a concentration of 0.45 and 1.04 mg/mL did not decrease the cell viability in LM2 cells compared to the control cells. The minimum PANI-Nps' concentration to decrease significantly cell viability (71.7 %) was 2.94 mg/mL, while a concentration of 7.5 mg/mL decreased cell viability even more (39 %). The highest concentration directly tested (12 mg/mL) did not allow colony formation in LM2 cells. The results of this study demonstrated that MTT assay could be implemented as an effective and sensitive tool to assess PANI-Nps' cytotoxicity on tumor cell lines.

Cell viability by the Tripan blue exclusion assay (Fig. 4b) showed that PANI-Nps are not toxic for a Murine mammary adenocarcinome cell line, confirming the results obtained by MTT and neutral red assay at these concentrations. High concentrations of nanoparticles were required to obtain the cytotoxicity assuming the safety of nanoparticles to be used therapeutically at lower concentrations. Microscopic observations by toluidine blue staining of control cells (Fig. 5a) and nanoparticle-treated cells (Fig. 5b) did not show alteration in cell shape or morphology in a monolayer culture indicating healthy cells. Furthermore, cells incubated with a media containing the stabilizer PVP appeared similar to control cells (Fig. 5d). These results suggest the innocuousness of PANI nanoparticles and the polymer stabilizer at concentrations lower than 1.5 mg/mL of PANI-Nps, and as a consequence, to determinate photothermal effects of PANI-Nps, concentrations lower than 1.5 mg/mL were employed with laser treatment.

Laser treatment of tumor cells with PANI-Nps

Cells irradiated with NIR laser in the absence of nanoparticles at different periods or incubated with PVP and irradiated did not show cell death or alteration in cell morphology (Fig. 5c, e, respectively). On the contrary, cells incubated with 1.04 mg PANI-Nps/mL and irradiated with NIR laser light for 15 min (Fig. 5f, g) showed changes in cell phenotype with apoptosis as a mechanism of cell death, and also cell detachment and debris were observed, suggesting a necrotic mechanism of cell death. PANI-Np (1.04 mg/mL)-treated cells showed an apoptosis morphology. This finding was observed at different doses of irradiation, being more pronounced especially at 15 min of illumination. Apoptosis is defined as a distinct set of morphological changes observed during cell death, including the formation of cell membrane buds or blebs, and a decrease in total cell volume (Hurle and Merino 1999; Häcker 2000). Furthermore, using AFM, changes in the cellular morphology between cells treated with nanoparticles and irradiated and control cells were also

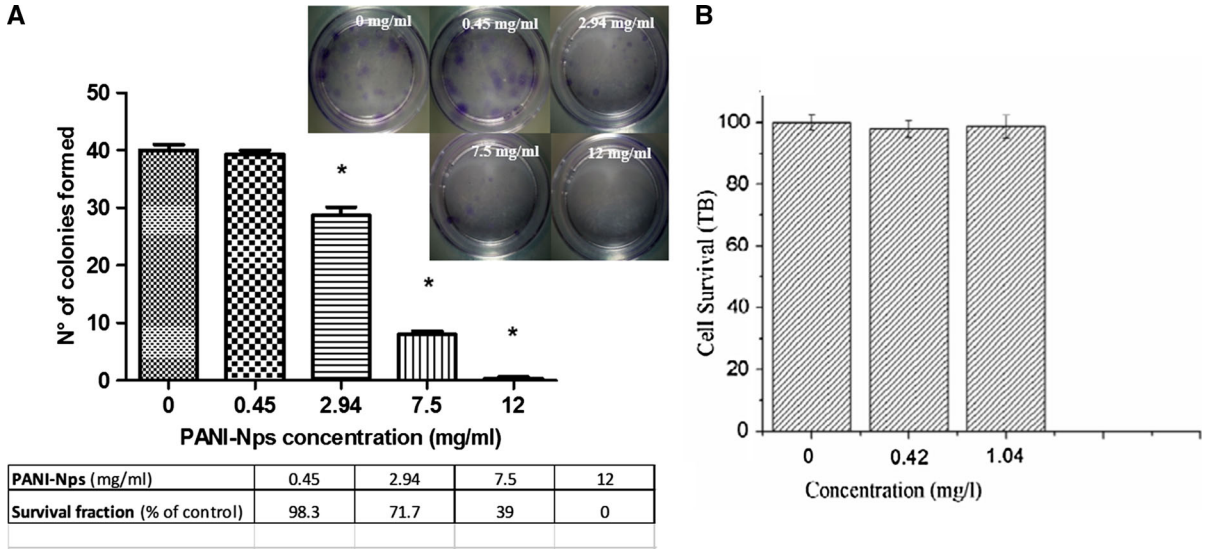

PANI-Nps (mg/ml)	0.45	2.94	7.5	12
Survival fraction (% of control)	98.3	71.7	39	0

Fig. 4 **a** Effects of PANI-Nps at different concentrations on cell viability evaluated by colony-formation assay after 24 h of exposure to nanoparticles and followed by 10 days, and **b** effects of PANI-Nps (0.42 and 1.04 mg/mL) after 24-h exposure in dark condition on cell viability using Tripan Blue staining

observed (Fig. 6). The images shown are a typical representation of these changes. The obvious morphological changes such as disappearance of filopodia, volume changes, and transformation to a round shape observed by AFM were consistent through three separate experiments only in the area of laser illumination (Wang et al. 2011b; Lee et al. 2013; Gaspar et al. 2015). These results suggest that the combination of nanoparticles and radiation triggers cell death by apoptosis in attached cells. Promising results with these nanoparticles were obtained in our laboratory for in vivo assays with apoptosis and necrosis as the responsible mechanisms of cell death (Ibarra et al. 2013). Previous studies of polyaniline nanoparticles in PTT showed similar results in different cancer cell lines (Yang et al. 2011; Zhou et al. 2013). Apparently, the uptakes of both PANI-Nps and the laser dosage are the controlling factors for thermally induced cytotoxicity.

PTT triggers oxidative stress

Based on the results obtained in the biochemical investigation, a status check of intracellular oxidative stress was done using DCFDA (2, 7-dichlorodihydrofluorescein diacetate) fluorescent dye. Cells irradiated in the presence or the absence of dispersant did not show ROS generation (Fig. 7). Cells treated only with PANI nanoparticles in dark condition did not exhibit oxidative stress. On the contrary, Xue et al. demonstrated that nano-Cu affected the oxidant–antioxidant balance and induced cytotoxicity in podocytes, resulting in the enhanced generation of ROS. These results suggested that oxidative stress played an important role in the mechanism of nano-Cu toxicity in podocytes (Xu et al. 2012). Similar behavior has been observed for different nanoparticles in cultured cells (Pulskamp et al. 2007; Park and Park 2009; Passagne et al. 2012). However, this seems not to be the case for PANI-Np. In fact, Kucekova et al. report that exposure of neutrophil leukocytes to PANI-Nps <150 μg/mL did not only produce ROS, but they could also act as ROS scavengers (Kucekova et al. 2014). In our study, however, we found that the cells that are treated with PANI-Nps (0.42 and 1.04 mg/mL) and irradiated lead to ROS generation, which could be sensed from DCF fluorescence (Fig. 7). These results indicated that intracellular oxidation is occurring during PTT. Mitochondria are the potential sites of ROS production in cells, and thus, considered the major sites of generation of oxidative stress after injuring the organelle (Hiura et al. 2000). Recently, different studies have reported that nanoparticles with

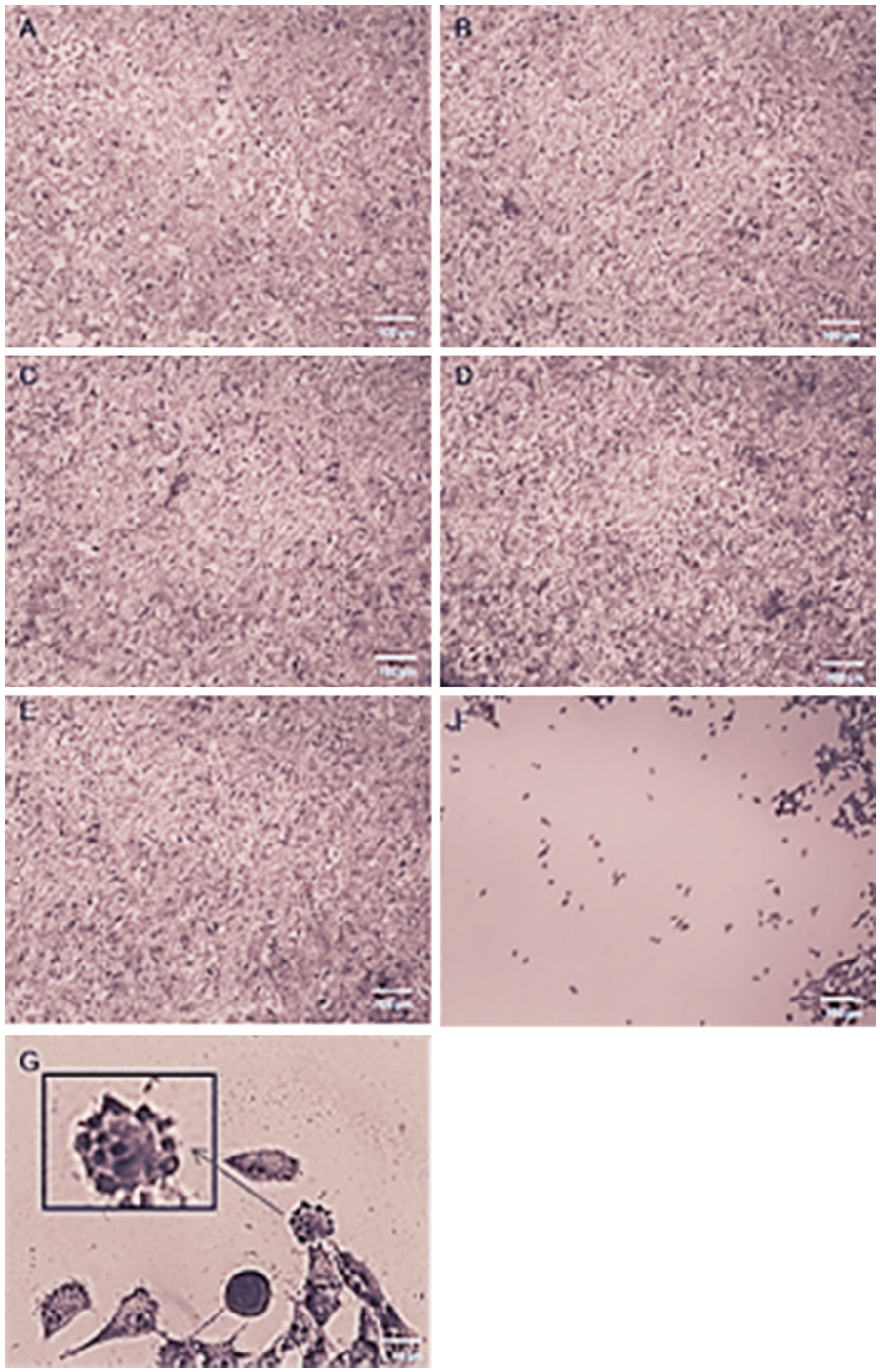

Fig. 5 Images of LM2 cells staining with Toluidine blue obtained by inverted-design optical microscope (×10 magnification). **a** Control cells, **b** cells incubated with 1.04 mg PANI-Nps/mL (*dark control*), **c** cells irradiated with NIR laser light for 15 min (*light control*), **d** cells incubated with stabilizer PVP, **e** cells incubated with PVP and irradiated with NIR laser light for 15 min, **f** cells incubated with 1.04 mg PANI-Nps/mL and irradiated with NIR laser light for 15 min, **g** cells incubated with 1.04 mg PANI-Nps/mL and irradiated with NIR laser light for 15 min

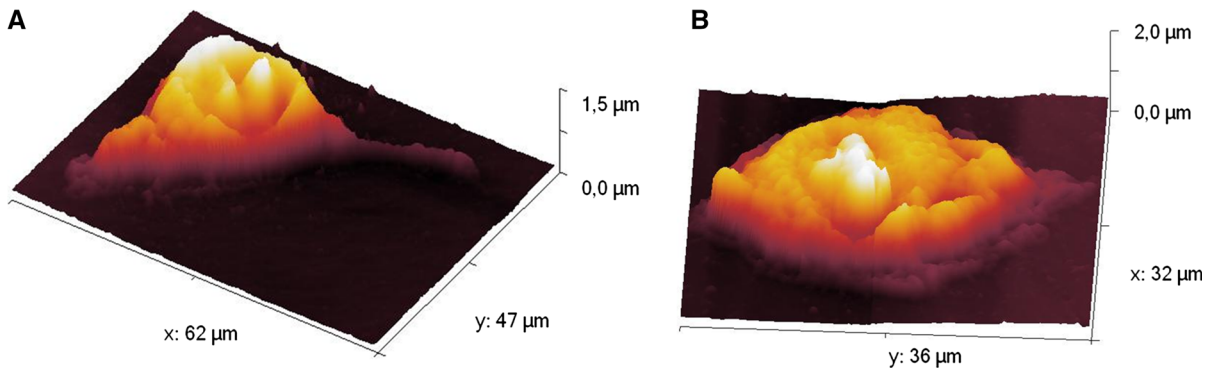

Fig. 6 AFM microscopy images of LM2 cells. **a** Control cell and **b** cells incubated with 1.04 mg PANI-Nps/mL and irradiated with NIR laser light for 15 min

different sizes and chemical compositions can be localized near the mitochondria in tumor cells, and therefore induce major structural damage that would cause the generation of ROS after PTT (Markovic et al. 2011; Mocan et al. 2014). In addition, exposure to high temperature for a sufficient amount of time causes physical damage such as protein denaturation and membrane lysis, and can increase oxidative stress (Jaque et al. 2014). We suggest that mitochondria could be a secondary target of PTT like other organelles such as lysosomes, and therefore the damages to these structures may alter the oxidative balance of cells. PANI-Nps is released into the cytoplasm of LM2 cells by endocytosis and could be translocated from endosomes/lysosomes to mitochondria, inducing a decrease in the mitochondrial membrane potential and an increase in the oxidation stress, and finally triggering cell death. The increase of intracellular ROS by hyperthermia could be considered to be a likely mechanism for hyperthermia-induced cell injury and the principle of hyperthermic treatment in cancer therapy. This effect is related to a mild hyperthermia achieved in tumor cells (41–45 °C) that induce apoptosis, and higher temperatures (>45 °C) inducing a necrotic cell death (Ahmed and Zaidi 2013; Purschke et al. 2010). Seemingly in our study, cells from the inner center suffer death due to necrosis, and then they get detached from the substrate; on the other hand, cells from the periphery, which achieve a moderate temperature, die due to apoptosis. Mocan et al. (2014) confirmed this result showing that mitochondrial membrane permeabilization with consequent apoptosis represents the primary mode of death induction following administration of MWCNTs-PEG combined with laser irradiation by activating early apoptosis pathways. Zhang et al. (2014) reported that EGFRmAb-AuNRs, with appropriate laser irradiation, resulted in higher Hep-2 cells apoptosis in vitro, accompanied by alteration of reactive oxygen species (ROS) production, Ca^{2+} release, and change in mitochondrial membrane potential ($\Delta\Psi m$). The data suggested that the apoptosis induced by EGFRmAb-AuNRs was ROS-dependent, and that ROS generation might be required for subsequent activations of apoptotic factors, like caspase-3. Previous reports demonstrated that hyperthermia was associated with the increases of intracellular reactive oxygen species (ROS) and apoptosis in U-2 OS cells. In addition, hyperthermia triggered the endoplasmic reticulum (ER) stress, which was characterized by changes in cytosolic calcium levels, as well as increased calpain expression and activity. In conclusion, hyperthermia induced cell apoptosis substantially via the ROS, ER stress, mitochondria, and caspase pathways (Hou et al. 2014). In addition, Yoo et al. (2012), demonstrated that ROS-generating magnetic nanoparticles can effectively sensitize cancer cells to make them highly vulnerable to subsequent apoptotic magnetic hyperthermia at low temperatures (43 °C). The increase of intracellular ROS by hyperthermia could be considered a probable mechanism for hyperthermia-induced cell injury in cancer therapy.

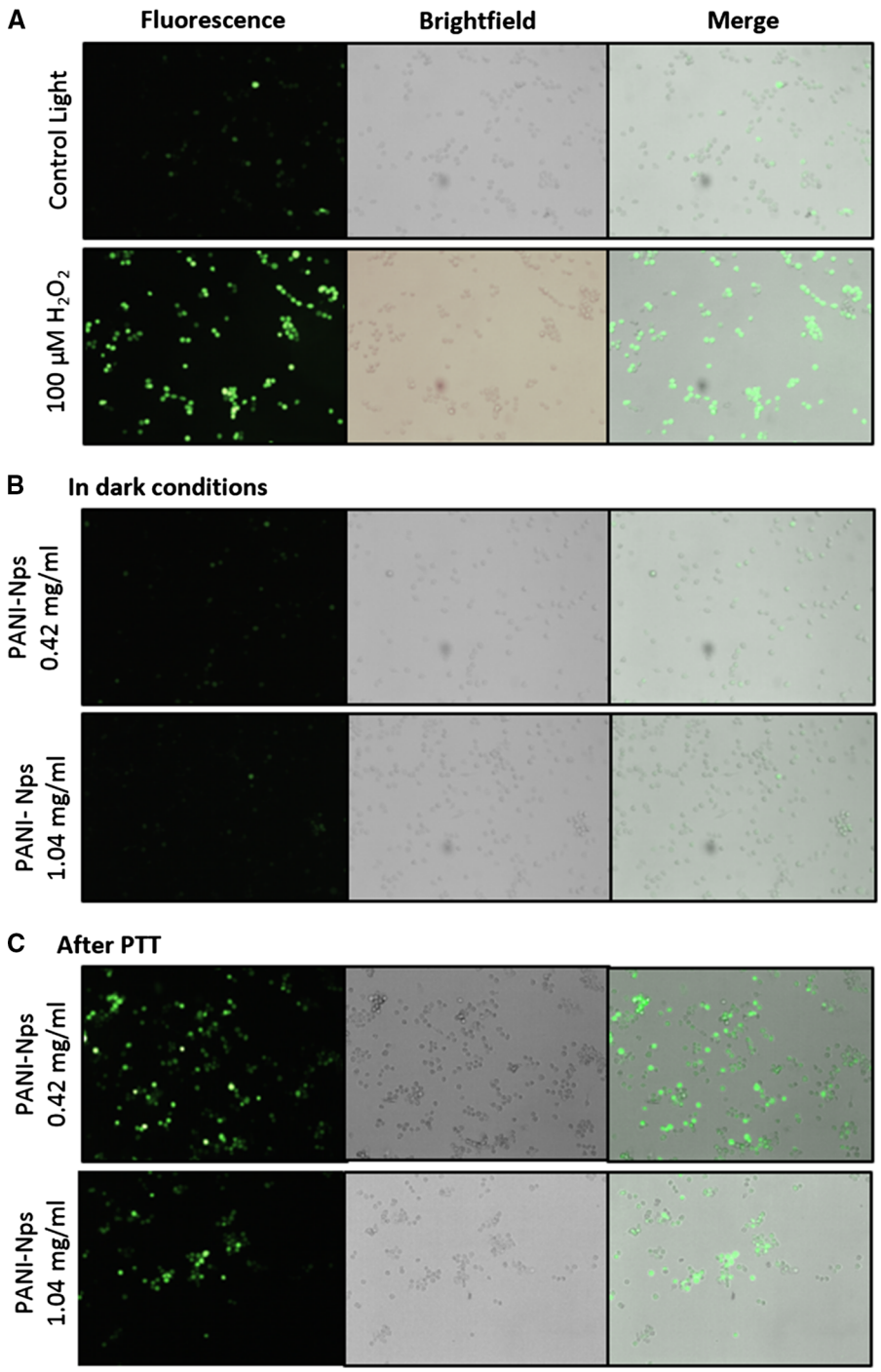

Fig. 7 Fluorescence images of ROS captured 60 min after PTT treatment. **a** Positive control cells incubated with 100 μM H_2O_2 for 2 h and cells only irradiated with laser NIR for 15 min (negative control), **b** PANI-Nps exposure at 0.42 and 1.04 mg/mL for 24 h under dark condition, and **c** PTT treatment of cells with PANI-Nps at 0.42 and 1.04 mg/mL and irradiated with NIR laser for 15 min. Each *green spot* corresponds to a single cell producing ROS

Conclusions

In this study, the incorporation kinetic of PANI-Nps in LM2 cell was evaluated at different exposure times, and a significant decrease in the cellular uptake at lower temperature (4 °C) compared to 37 °C involving the participation of an endocytic mechanism was observed. Furthermore, the cell viabilities in the wells treated with concentrations lower than 1.5 mg/mL of PANI-Nps in dark conditions were comparable to those of control cells. Microscopic observation of cells treated with nanoparticles in the absence of light or those only irradiated showed no indication of any morphological change and cell death. The PANI-Nps were biocompatible, and did not show cytotoxicity to cells.

In contrast, the combination of laser in the near-infrared region (NIR) and PANI-Nps induced cell death. These results suggest that oxidative stress played an important role leading to apoptosis-induced cell death post-PTT with this type of nanoparticles. In conclusion, the PANI-Nps show promise as a new therapeutic agent in this regime, because this nanomaterial is capable of inducing selective photothermal destruction of cancer cells by laser-nanoparticle treatment. We suggest that cell death could be attributed to a synergistic effect of hyperthermia-induced cell necrosis (detachment cell) and heat diffusion/ROS migration-caused apoptosis (attach cell).

Acknowledgments The authors are grateful to the Secretaría de Ciencia y Técnica (SECYT) of Universidad Nacional de Río Cuarto and Consejo Nacional de Investigaciones Científicas y Técnicas (CONICET) for their financial support. L. Ibarra thanks CONICET for a research fellowship. V. Rivarola, C. Barbero, and E.I. Yslas hold the posts as Scientific Researchers at the CONICET. The authors also are thankful to Dr. Diego Acevedo for the images of AFM microscopy.

References

Acevedo DA, Lasagni AF, Barbero CA, Mücklich F (2007) Simple fabrication method of conductive polymeric arrays by using direct laser interference micro-/nanopatterning. Adv Mater 19:1272–1275. doi:10.1002/adma.200601693

Ahmed K, Zaidi SF (2013) Treating cancer with heat: hyperthermia as promising strategy to enhance apoptosis. J Pak Med Assoc 63:504–508

Allison SD (2007) Liposomal drug delivery. J Infus Nurs 30:89–95. doi:10.1097/01.NAN.0000264712.26219.67

Balasubramanian SK, Jittiwat J, Manikandan J et al (2010) Biodistribution of gold nanoparticles and gene expression changes in the liver and spleen after intravenous administration in rats. Biomaterials 31:2034–2042. doi:10.1016/j.biomaterials.2009.11.079

Bovis MJ, Woodhams JH, Loizidou M et al (2012) Improved in vivo delivery of m-THPC via pegylated liposomes for use in photodynamic therapy. J Control Release 157:196–205. doi:10.1016/j.jconrel.2011.09.085

Casas A, Perotti C, Saccoliti M et al (2002) ALA and ALA hexyl ester in free and liposomal formulations for the photosensitisation of tumour organ cultures. Br J Cancer 86:837–842. doi:10.1038/sj.bjc.6600144

Choi EB, Choi J, Bae SR et al (2014) Colourimetric redox-polyaniline nanoindicator for in situ vesicular trafficking of intracellular transport. Nano Res. doi:10.1007/s12274-014-0597-6

Chu M, Shao Y, Peng J et al (2013) Near-infrared laser light mediated cancer therapy by photothermal effect of Fe_3O_4 magnetic nanoparticles. Biomaterials 34:4078–4088. doi:10.1016/j.biomaterials.2013.01.086

Fery-Forgues S (2013) Fluorescent organic nanocrystals and non-doped nanoparticles for biological applications. Nanoscale 5:8428–8442. doi:10.1039/c3nr02657d

Fu G, Liu W, Feng S, Yue X (2012) Prussian blue nanoparticles operate as a new generation of photothermal ablation agents for cancer therapy. Chem Commun 48:11567–11569. doi:10.1039/c2cc36456e

Gaspar D, Freire JM, Pacheco TR et al (2015) Apoptotic human neutrophil peptide-1 anti-tumor activity revealed by cellular biomechanics. Biochim Biophys Acta 1853:308–316. doi:10.1016/j.bbamcr.2014.11.006

Häcker G (2000) The morphology of apoptosis. Cell Tissue Res 301:5–17

Haley B, Frenkel E (2008) Nanoparticles for drug delivery in cancer treatment. Urol Oncol 26:57–64. doi:10.1016/j.urolonc.2007.03.015

Heeger AJ (1993) Polyaniline with surfactant counterions: conducting polymer materials which are processible in the conducting form. Synth Met 57:3471–3482. doi:10.1016/0379-6779(93)90462-6

Hiura TS, Li N, Kaplan R et al (2000) The role of a mitochondrial pathway in the induction of apoptosis by chemicals extracted from diesel exhaust particles. J Immunol 165:2703–2711

Hong C, Lee J, Zheng H et al (2011) Porous silicon nanoparticles for cancer photothermotherapy. Nanoscale Res Lett 6:321. doi:10.1186/1556-276X-6-321

Hou C-H, Lin F-L, Hou S-M, Liu J-F (2014) Hyperthermia induces apoptosis through endoplasmic reticulum and reactive oxygen species in human osteosarcoma cells. Int J Mol Sci 15:17380–17395. doi:10.3390/ijms151017380

Huang N, Wang H, Zhao J et al (2010) Single-wall carbon nanotubes assisted photothermal cancer therapy: animal study with a murine model of squamous cell carcinoma. Lasers Surg Med 42:638–648. doi:10.1002/lsm.20968

Hurle JM, Merino R (1999) When Cells Die: A Comprehensive Evaluation of Apoptosis and Programmed Cell Death (1998). Lockshin RA, Zakeri Z, Tilly JL (eds). New York: Wiley-Liss, 504 pp. £65 hardback; ISBN 0-471-16569-7. BioEssays 21:92–92. doi: 10.1002/(SICI)1521-1878(199901)21:1<92::AID-BIES15>3.0.CO;2-U

Ibarra LE, Yslas EI, Molina MA et al (2013) Near-infrared mediated tumor destruction by photothermal effect of

PANI-Np in vivo. Laser Phys 23:066004. doi:10.1088/1054-660X/23/6/066004

Ibarra LE, Tarres L, Bongiovanni S et al (2015) Assessment of polyaniline nanoparticles toxicity and teratogenicity in aquatic environment using *Rhinella arenarum* model. Ecotoxicol Environ Saf 114:84–92. doi:10.1016/j.ecoenv.2015.01.013

Jaque D, Maestro LM, del Rosal B et al (2014) Nanoparticles for photothermal therapies. Nanoscale. doi:10.1039/C4NR00708E

Kampinga HH (2006) Cell biological effects of hyperthermia alone or combined with radiation or drugs: a short introduction to newcomers in the field. Int J Hyperth 22:191–196. doi:10.1080/02656730500532028

Kievit FM, Veiseh O, Bhattarai N et al (2009) PEI–PEG–chitosan copolymer coated iron oxide nanoparticles for safe gene delivery: synthesis, complexation, and transfection. Adv Funct Mater 19:2244–2251. doi:10.1002/adfm.200801844

Kucekova Z, Humpolicek P, Kasparkova V et al (2014) Colloidal polyaniline dispersions: antibacterial activity, cytotoxicity and neutrophil oxidative burst. Colloids Surf B Biointerfaces 116:411–417. doi:10.1016/j.colsurfb.2014.01.027

Kumari A, Yadav SK, Yadav SC (2010) Biodegradable polymeric nanoparticles based drug delivery systems. Colloids Surf B Biointerfaces 75:1–18. doi:10.1016/j.colsurfb.2009.09.001

Lee ES, Na K, Bae YH (2003) Polymeric micelle for tumor pH and folate-mediated targeting. J Control Release 91:103–113

Lee ES, Gao Z, Bae YH (2008) Recent progress in tumor pH targeting nanotechnology. J Control Release 132:164–170. doi:10.1016/j.jconrel.2008.05.003

Lee YJ, Lee G-J, Kang SW et al (2013) Label-free and quantitative evaluation of cytotoxicity based on surface nanostructure and biophysical property of cells utilizing AFM. Micron 49:54–59. doi:10.1016/j.micron.2013.02.014

Li K, Liu B (2014) Polymer-encapsulated organic nanoparticles for fluorescence and photoacoustic imaging. Chem Soc Rev. doi:10.1039/c4cs00014e

Li D, Huang J, Kaner RB (2009) Polyaniline nanofibers: a unique polymer nanostructure for versatile applications. Acc Chem Res 42:135–145. doi:10.1021/ar800080n

Markovic ZM, Harhaji-Trajkovic LM, Todorovic-Markovic BM et al (2011) In vitro comparison of the photothermal anticancer activity of graphene nanoparticles and carbon nanotubes. Biomaterials 32:1121–1129. doi:10.1016/j.biomaterials.2010.10.030

Marquis BJ, Love SA, Braun KL, Haynes CL (2009) Analytical methods to assess nanoparticle toxicity. Analyst 134:425–439. doi:10.1039/b818082b

Mocan T, Matea CT, Cojocaru I et al (2014) Photothermal treatment of human pancreatic cancer using PEGylated multi-walled carbon nanotubes induces apoptosis by triggering mitochondrial membrane depolarization mechanism. J Cancer 5:679–688. doi:10.7150/jca.9481

Ngamna O, Morrin A, Killard AJ et al (2007) Inkjet printable polyaniline nanoformulations. Langmuir 23:8569–8574. doi:10.1021/la700540g

Novák P, Müller K, Santhanam KSV, Haas O (1997) Electrochemically active polymers for rechargeable batteries. Chem Rev 97:207–282

Park E-J, Park K (2009) Oxidative stress and pro-inflammatory responses induced by silica nanoparticles in vivo and in vitro. Toxicol Lett 184:18–25. doi:10.1016/j.toxlet.2008.10.012

Passagne I, Morille M, Rousset M et al (2012) Implication of oxidative stress in size-dependent toxicity of silica nanoparticles in kidney cells. Toxicology 299:112–124. doi:10.1016/j.tox.2012.05.010

Pulskamp K, Diabaté S, Krug HF (2007) Carbon nanotubes show no sign of acute toxicity but induce intracellular reactive oxygen species in dependence on contaminants. Toxicol Lett 168:58–74. doi:10.1016/j.toxlet.2006.11.001

Purschke M, Laubach H-J, Anderson RR, Manstein D (2010) Thermal injury causes DNA damage and lethality in unheated surrounding cells: active thermal bystander effect. J Investig Dermatol 130:86–92. doi:10.1038/jid.2009.205

Royall JA, Ischiropoulos H (1993) Evaluation of 2′,7′-dichlorofluorescin and dihydrorhodamine 123 as fluorescent probes for intracellular H_2O_2 in cultured endothelial cells. Arch Biochem Biophys 302:348–355. doi:10.1006/abbi.1993.1222

Schulze C, Kroll A, Lehr C-M et al (2008) Not ready to use—overcoming pitfalls when dispersing nanoparticles in physiological media. Nanotoxicology 2:51–61. doi:10.1080/17435390802018378

Shevach M, Fleischer S, Shapira A, Dvir T (2014) Gold nanoparticle-decellularized matrix hybrids for cardiac tissue engineering. Nano Lett 14:5792–5796. doi:10.1021/nl502673m

Sokolova V, Kozlova D, Knuschke T et al (2013) Mechanism of the uptake of cationic and anionic calcium phosphate nanoparticles by cells. Acta Biomater 9:7527–7535. doi:10.1016/j.actbio.2013.02.034

Stejskal J, Proke J (2014) Reprotonated polyanilines: the stability of conductivity at elevated temperature. Polym Degrad Stab 102:67–73. doi:10.1016/j.polymdegradstab.2014.02.001

Stejskal J, Sapurina I (2005) Polyaniline: thin films and colloidal dispersions (IUPAC Technical Report). Pure Appl Chem 77:815–826. doi:10.1351/pac200577050815

Stejskal J, Hajná M, Kašpárková V et al (2014) Purification of a conducting polymer, polyaniline, for biomedical applications. Synth Met 195:286–293. doi:10.1016/j.synthmet.2014.06.020

Stern ST, Adiseshaiah PP, Crist RM (2012) Autophagy and lysosomal dysfunction as emerging mechanisms of nanomaterial toxicity. Part Fibre Toxicol 9:20. doi:10.1186/1743-8977-9-20

Sultan RA (1990) Tumour ablation by laser in general surgery. Lasers Med Sci 5:185–193. doi:10.1007/BF02031380

Thurn KT, Arora H, Paunesku T et al (2011) Endocytosis of titanium dioxide nanoparticles in prostate cancer PC-3M cells. Nanomedicine 7:123–130. doi:10.1016/j.nano.2010.09.004

Verma A, Stellacci F (2010) Effect of surface properties on nanoparticle-cell interactions. Small 6:12–21. doi:10.1002/smll.200901158

Villalba P, Ram MK, Gomez H et al (2012) Cellular and in vitro toxicity of nanodiamond-polyaniline composites in mammalian and bacterial cell. Mater Sci Eng, C 32:594–598. doi:10.1016/j.msec.2011.12.017

Virji S, Huang J, Kaner RB, Weiller BH (2004) Polyaniline nanofiber gas sensors: examination of response mechanisms. Nano Lett 4:491–496. doi:10.1021/nl035122e

Wang C, Cheng L, Liu Z (2011a) Drug delivery with upconversion nanoparticles for multi-functional targeted cancer cell imaging and therapy. Biomaterials 32:1110–1120. doi:10.1016/j.biomaterials.2010.09.069

Wang D-C, Chen K-Y, Tsai C-H et al (2011b) AFM membrane roughness as a probe to identify oxidative stress-induced cellular apoptosis. J Biomech 44:2790–2794. doi:10.1016/j.jbiomech.2011.08.021

Weissleder R (2001) A clearer vision for in vivo imaging. Nat Biotechnol 19:316–317. doi:10.1038/86684

Welch A (1984) The thermal response of laser irradiated tissue. IEEE J Quantum Electron 20:1471–1481. doi:10.1109/JQE.1984.1072339

Xu P, Xu J, Liu S, Yang Z (2012) Nano copper induced apoptosis in podocytes via increasing oxidative stress. J Hazard Mater 241–242:279–286. doi:10.1016/j.jhazmat.2012.09.041

Yang J, Choi J, Bang D et al (2011) Convertible organic nanoparticles for near-infrared photothermal ablation of cancer cells. Angew Chem Int Ed Engl 50:441–444. doi:10.1002/anie.201005075

Yoo D, Jeong H, Preihs C et al (2012) Double-effector nanoparticles: a synergistic approach to apoptotic hyperthermia. Angew Chem Int Ed Engl 51:12482–12485. doi:10.1002/anie.201206400

Yslas EI, Ibarra LE, Peralta DO et al (2012) Polyaniline nanofibers: acute toxicity and teratogenic effect on *Rhinella arenarum* embryos. Chemosphere 87:1374–1380. doi:10.1016/j.chemosphere.2012.02.033

Yuan H, Khoury CG, Wilson CM et al (2012) In vivo particle tracking and photothermal ablation using plasmon-resonant gold nanostars. Nanomedicine. doi:10.1016/j.nano.2012.02.005

Zhang X, Wu D, Zhao B et al (2011) Size-dependent in vivo toxicity of PEG-coated gold nanoparticles. Int J Nanomedicine 6:2071–2081

Zhang S, Li Y, He X et al (2014) Photothermolysis mediated by gold nanorods modified with EGFR monoclonal antibody induces Hep-2 cells apoptosis in vitro and in vivo. Int J Nanomedicine 9:1931–1946. doi:10.2147/IJN.S59870

Zhao J, Zhou R, Fu X et al (2014) Cell-penetrable lysine dendrimers for anti-cancer drug delivery: synthesis and preliminary biological evaluation. Arch Pharm 347:469–477. doi:10.1002/ardp.201300415

Zhou J, Lu Z, Zhu X et al (2013) NIR photothermal therapy using polyaniline nanoparticles. Biomaterials 34:9584–9592. doi:10.1016/j.biomaterials.2013.08.075